Non-Local Transport in Turbulent MHD Convection

Mark Miesch[2,3] Axel Brandenburg[1], Ellen Zweibel[2,3], and Juri Toomre[2,3]

[1] NORDITA, Blegdamsvej 17, DK-2100 Copenhagen Ø, Denmark
[2] Joint Institute for Laboratory Astrophysics, University of Colorado, Boulder, CO 80309-0440

ABSTRACT

The nonlocal, non-diffusive transport of passive scalars in turbulent MHD convection is investigated using transilient matrices, which describe the "probability" that a tracer particle beginning at one position in a flow will be advected to another position after some time. We present a new method for calculating these matrices from simulation data which involves following the trajectories of passive tracer particles and calculating their transport statistics. The method is applied to study transport in several simulations of turbulent, rotating, three dimensional, compressible, penetrative MHD convection. Transport coefficients and other useful diagnostics such as moments of the transilient matrix are used to quantify the transport, which is found to resemble advection more closely than diffusion. Some of the results also have direct relevance for other physical problems, such as light element depletion in solar-type stars. In particular the large kurtosis found for downward moving particles at the base of the convection zone implies a relatively large number of extreme events - particles traveling deep into the radiative interior where light elements would be efficiently burned.

1. INTRODUCTION

When describing the transport of chemical species (passive tracers) in turbulent flows, it is often assumed that the process is diffusive in nature, with an enhanced "eddy diffusivity" which is much larger than that due solely to molecular diffusion. However, such a prescription is based on the central limit theorem, and is invalid for systems which possess broad distribution functions or large scale correlations in the velocity field (Bouchaud & Georges 1990). Since convective plumes and other coherent structures often play an important role in astrophysical and geophysical flows, classical diffusion is often not applicable (although it is often employed), and more general formulations are necessary to accurately describe the transport of passive tracer particles. Stull and colleagues (reviewed by Stull 1993; see also Ebert *et al.* 1989) have developed such a formulation for use in describing the transport characteristics of turbulent convection in the earth's atmosphere. Rather than considering an expansion of particle fluxes in terms of local derivatives of the particle concentrations, they instead quantify transport by means of "transilient", or "probability" matrices, which are related to Green's functions and which describe the probability that a particle beginning at some position in the flow will end up at another particular position after a specified time interval. Although other descriptions of non- diffusive transport do exist (reviewed by Stull 1993), the transilient matrix approach has the advantage that it's straightforward to calculate for a given velocity field, it's relatively easy to interpret, and it provides a wealth of information on the large and small scale mixing properties of the flow. In the present work, we use the transilient matrix framework to describe the non-diffusive, non-local transport of tracer particles in simulations of turbulent, compressible, rotating, three-dimensional, MHD convection with overshoot. Two different resolutions were used, the first being 63^3, and the second $126^2 \times 105$ (see Brandenburg *et al.* 1995a for a description of the simulations).

Understanding and quantifying mixing processes in simulation data, will help to interpret future helioseismological data on elemental abundances and distributions. A more detailed account of the present work will be presented elsewhere (Brandenburg *et al* 1995b).

2. THE TRANSILIENT MATRIX APPROACH

The concentration per unit mass of a chemical species passively advected by a flow in the absence of molecular diffusion evolves according to the equation

$$\frac{Dc}{Dt} = 0, \tag{1.1}$$

where D/Dt denotes the Lagrangian derivative, $\partial/\partial t + u \cdot \nabla$. In what follows, we are primarily concerned with vertical transport, so it is of interest to consider the horizontally averaged particle concentration as a function of depth and time, $\bar{c}_i(t)$, which can be written as follows:

$$\bar{c}_i(t) = \sum_j G_{ij}(t)\bar{c}_j(0) \tag{1.2}$$

where G_{ij} is in effect a Green's function which describes the response of the system to an injection of particles on level j. We hereafter refer to G_{ij} as the "transilient" matrix for the flow, after Stull (1993). Note that since c is the concentration per unit mass (satisfying equation 1.1), the levels i and j must be chosen to be of constant mass and their spatial width must therefore vary if the fluid is stratified in the vertical (z) direction. In some instances, it is also useful to consider levels, or bins, of constant volume (see below), although the transport in this case is dominated by a net downward motion of particles until their mean concentration matches the stratification. Unless otherwise noted, constant mass bins will be used for the present work.

In practice, we calculate the matrix G_{ij} by injecting particles into simulations of turbulent MHD convection after it has evolved to a statistically steady state. The particle trajectories are then calculated (using either a time-independent "snapshot" of the velocity field, or one that includes the full time dependence), and their statistics then give a direct measure of the transilient matrix. This is more computationally efficient, but less rigorous than the procedure originally developed by Stull and colleagues which involves the solution of a differential equa-

3 Also Department of Astrophysical, Planetary, and Atmospheric Sciences, University of Colorado, Boulder

Proceedings of Fourth SOHO Workshop: Helioseismology, Pacific Grove, California, 2–6 April 1995 (ESA SP-376, June 1995)

tion for a scalar field at each initial level, following a large eddy simulation model. The simulations used here have been presented and analyzed elsewhere (Brandenburg *et al.* 1995a) and are intended to model rotating, compressible, stratified, MHD, turbulent, penetrative convection in solar-type stars, but the method and results presented here are of general interest in understanding and quantifying transport in convective turbulence.

A sample slice along one of the columns of the transilient matrix for the simulations is shown in Figure 1. These plots were made using bins of constant volume and correspond to the higher resolution run, including the full time dependence of the flow (i.e. the fully compressible MHD equations were solved to evolve the velocity field in time after the addition of the tracer particles), although the steady state version (i.e. using only a time-independent "snapshot" of the velocity field) looks similar. The z coordinate (depth) is opposite to gravity, so the convectively unstable region lies below $z = 1$, while $z > 1$ corresponds to the convectively stable region underneath. Note the asymmetric spread away from the dashed line, which represents the initial state. Although the peak concentration arising from a source level is usually advected upward, the downward moving particles tend to propagate away from the diagonal more quickly, characteristic of the broad upflows and relatively strong, narrow downflows typically seen in compressible, stratified convection.

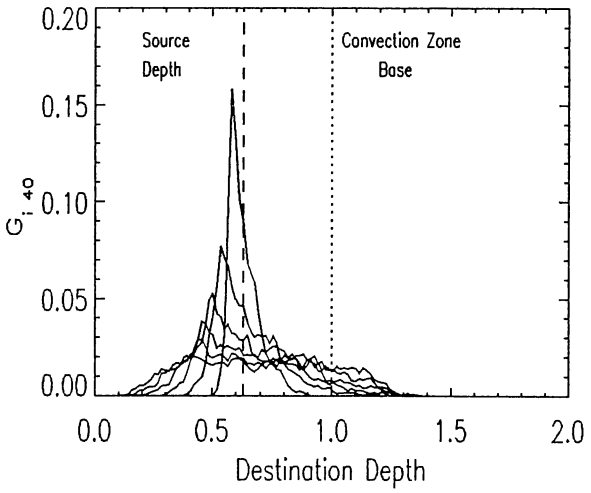

Figure 1. A cross section through the transilient matrix for the $126^2 \times 105$ resolution run for $t = 2.3$ to 13.8, in increments of 2.3, using bins of constant volume. The concentration begins as a delta function at the source depth, marked with a dotted line, and the progressively more disperse curves correspond to later times. The base of the convection zone is marked with a dotted line.

The horizontal averaging in equation (1.2) is only strictly valid if the initial concentration, $c(x, y, z, 0)$ is independent of x and y. Homogeneity in the horizontal directions is also necessary if the matrix is to have any predictive capabilities. That is, if one wishes to calculate the transilient matrix at a later time, formally we have

$$\bar{c}_i(t + \Delta t) = G_{ij}(t + \Delta t)\bar{c}_j(0) = G_{ij}(\Delta t)\bar{c}_j(t), \quad (1.3)$$

where the final equality treats $c_j(t)$ as an initial condition. But, since $\bar{c}_j(t) = G_{jk}(t)\bar{c}_k(0)$ (c.f. eqn 1.2), we have

$$G_{ij}(t + \Delta t) = G_{ik}(t)G_{kj}(\Delta t) \quad (1.4)$$

for a process which is statistically homogeneous in the horizontal directions. However, the horizontal averaging represents a loss of information about horizontal particle positions, so if significant inhomogeneities are present, such as those due to coherent structures, equation (1.4) breaks down. Note, however, that the transilient matrices presented here are exact in that the full three-dimensional dependence of particle trajectories is followed, and horizontal averaging is only performed when it comes time to compute the matrices.

A more general Green's function which depends on six spatial dimensions x, y, z, x', y', and z', is possible in principal, but memory requirements become prohibitively large unless some "coarse graining" is invoked. However, we can generalize the matrix to study horizontal transport without too much trouble if we include the average horizontal displacement as an extra dimension, i.e. if we consider $G_{\mu ij}(t)$, where μ is the root-mean-square horizontal displacement of a particle which begins on level j and ends up on level i after a time t. In practice, even the memory requirements for this reduced matrix are substantial, so here we only consider particular source levels, j, and use a more coarse binning for the destination levels (typically the destination bins for the horizontal matrix, $G_{\mu ij}$, contain 10 of the mass or volume levels used for the G_{ij} matrices, with one of the larger bins always centered around the source level, j).

3. DIAGNOSTICS

Several useful measures of nonlocal and local transport are readily available from the transilient matrix once it has been calculated for a given flow. The most straightforward are the various moments, and in particular, the second and and the normalized fourth order moments (variance and kurtosis) relative to the destination index, which are defined as

$$\sigma_j = \sum_i (z_i - z_j)^2 G_{ij} \quad (2.1)$$

and

$$\kappa_j = \frac{\sum_i (z_i - z_j)^4 G_{ij}}{\sigma_j^2}, \quad (2.2)$$

Because of the inherent anisotropy of the vertical transport, we generally split the moments up into upward and downward components and consider them separately. The square root of the variance is a measure of the typical mixing length (measured in *mass bins* if levels of constant mass are used) as a function of depth and time, and the kurtosis is a good quantitative descriptor of the shape of the distribution function (i.e. G_{ij}) as a function of time after an injection of particles on a given level.

The upward, downward, and horizontal variances as a function of time for the higher resolution run at a level within the convection zone are shown in Figure 2(a). The axes are logarithmic so the linear behavior (at least over some time interval) apparent in the plots implies a power law relationship of the form $\sigma^2 \sim t^\beta$. A similar power-law behavior is found for most levels, and the value of the best-fit exponents, β, as a function of depth are shown in Figure 2(b). The fits typically yield a value close to two, characteristic of advection rather than diffusion (which gives $\beta = 1$). The relatively large value of β for the downward variance near the top of the layer can be understood if the top layers are modeled as horizontal flows which converge into downward plumes. In this case, the time derivative of the mean downward displacement of particles originating on some level would be given approximately by the characteristic velocity of a plume, w_o, multiplied by the relative number of particles that have entered it - i.e. $d\sigma/dt \approx w_o(\pi(u_o t)^2 \Delta z c/N)$, where u_o is a characteristic horizontal velocity scale of the converging flow, N is the average number of particles in the level, Δz is the level's thickness, and c is the average particle concentration on that level per unit volume. Thus, σ would increase approximately as t^3, which would imply a β of 6. So, converging flows could be responsible for the tendency for β to increase near the top of the convection zone, where such flows may dominate the horizontal transport. The small values of the upward variance near the top can be attributed to the flattening of the $\sigma^2(t)$ curve as particles reach the top of the convection zone and turn around (see Fig. 2a). Similar results are found to hold for the lower resolution run, with the exception that the value of β for the upward variance near the top of the layer is significantly larger.

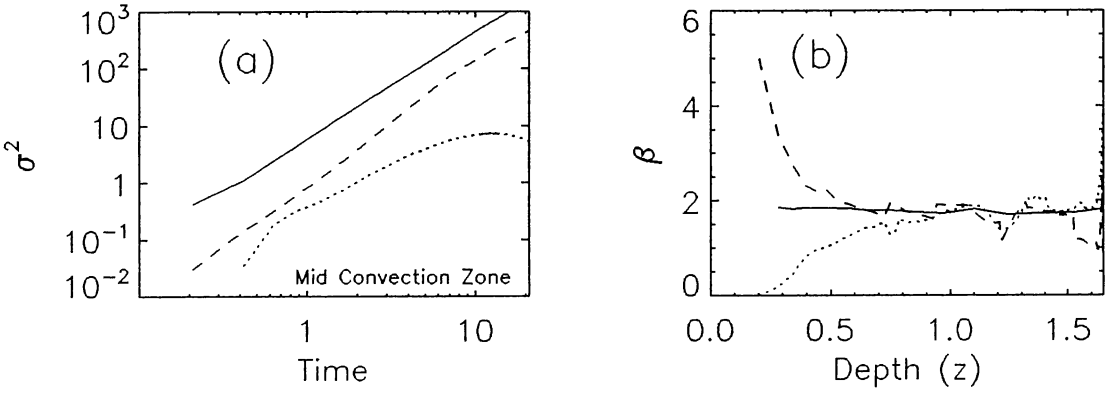

Figure 2. (a) The mean square upward (dotted line), downward (dashed line), and horizontal (solid line) particle displacement, or variance as a function of time for one particular level in the middle of the convection zone using the higher resolution data. Note the vertical displacements are given in terms of *mass levels*, which vary with depth but are comparable to the vertical grid spacing, while the horizontal variances are in terms of the horizontal grid spacing. (b) The best-fit power law exponents which satisfy $\sigma^2 \propto t^\beta$ as a function of depth, again for the higher resolution run, and again with the dotted, dashed, and solid lines corresponding to the upward, downward, and horizontal variances respectively.

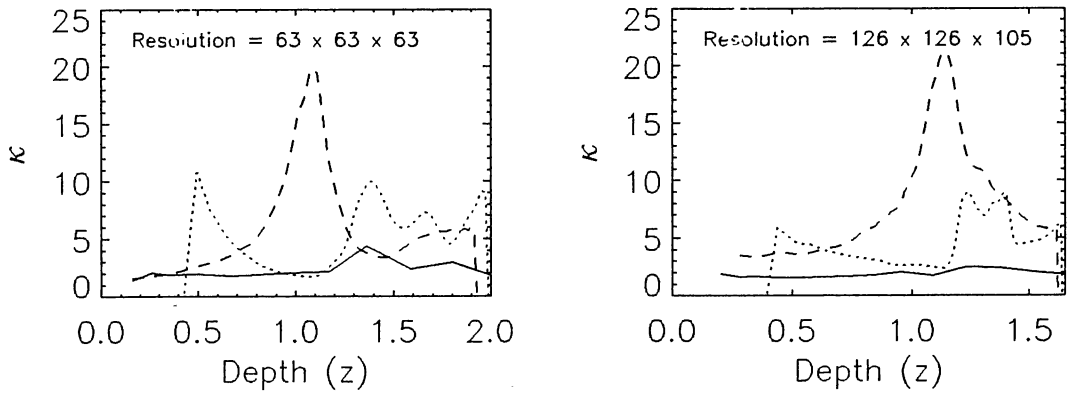

Figure 3. The kurtosis in the upward (dotted lines), downward (dashed lines), and horizontal (solid lines) directions are shown as a function of depth for both the higher and lower resolution runs at a time $t = 15$. The cutoffs for the upward kurtosis near the top of the convection zone are imposed because there are too few data points (< 5) there to give a reliable result.

The upward, downward, and horizontal kurtoses as a function of depth are shown in Figure 3. The kurtosis values, especially those in the horizontal and upward directions, are found to remain relatively constant in time. The layer corresponding to the plots in Figure 2(a), for example, shows a variation of the kurtoses of less than 25%, over a time range where the variances increase by three or four orders of magnitude (see Fig. 2a). The kurtoses therefore provide a useful quantitative measure for the shape of the matrix as it evolves away from the diagonal. The value $\kappa = 3$ is expected for diffusive processes and $\kappa = 1$ characterizes pure advection at a specific velocity. The large downward kurtoses just below the base of the convection zone indicate the relative importance of extreme events, wherein relatively few particles go on long excursions into the stable region below and enhance the tails of the distribution functions relative to the cores. Likewise, the upward kurtosis peaks below the convection zone, indicating the importance of long range mixing events relative to that expected for diffusion. This may have important implications for light element depletion in the Sun and similar stars.

Time derivatives of the moments of the Green's function can be used to derive transport coefficients and yield an expansion in terms of its local spatial derivatives. Following Van Beijeren (1982), we first write the fourier transform of the Green's function (written here as a continuous function for simplicity) as

$$\tilde{G}(k, z', t) = \int e^{-ik\zeta} G(\zeta, z', t) d\zeta =< e^{-ik\zeta} >, \tag{2.3}$$

where z' and z are the source and destination levels (corresponding to z_j and z_i above), $\zeta = z - z'$ and the angular brackets denote an average over all particles. The Greens function can then be expanded in a Taylor series and written as follows:

$$\tilde{G}(k, z', t) = \sum_{n=0}^{\infty} \frac{(-ik)^n}{n!} < \zeta^n >$$

$$= exp(\sum_{1}^{\infty} (ik)^n \chi_n / n!), \tag{2.4}$$

where the χ_n are cumulative moments (see Van Beijeren 1982):

$$\chi_1 = - < \zeta >$$
$$\chi_2 =< \zeta^2 > - < \zeta >^2 \tag{2.5}$$
$$\chi_3 = - < \zeta^3 > +3 < \zeta >< \zeta^2 > -2 < \zeta >^3$$
$$\ldots$$

Taking a time derivative and applying an inverse fourier transformation then yields:

$$\frac{\partial G(z, z', t)}{\partial t} = \sum_{n=1}^{\infty} T_n(z', t) \frac{\partial G(z, z', t)}{\partial z}, \tag{2.6}$$

where the transfer coefficients are given by

$$T_n = \frac{1}{n!} \frac{\partial \chi_n}{\partial t}. \tag{2.7}$$

Again, in the spirit of the Green's function formalism, an expansion in terms of these transport coefficients yields the particle fluxes that would arise in terms of local derivatives of the concentration if the initial concentration were a delta function at level z'. Thus, the time derivative of the concentration for an arbitrary initial condition is again a sum over all the individual contributions:

$$\frac{\partial \bar{c}(z, t)}{\partial t} = \int \sum T_n(z', t) \frac{\partial G(z, z', t) \bar{c}(z', 0)}{\partial z} dz', \tag{2.8}$$

and if the T_n are independent of depth, this reduces to the more familiar, but less general equation,

$$\frac{\partial \bar{c}(z, t)}{\partial t} = \sum_{n=1}^{\infty} T_n(t) \frac{\partial \bar{c}(z, t)}{\partial z}. \tag{2.9}$$

Similar relations also hold for horizontal transport, but note that the assumption of isotropy inherent in our approach implies that the only nonzero horizontal transport coefficients are those with n even.

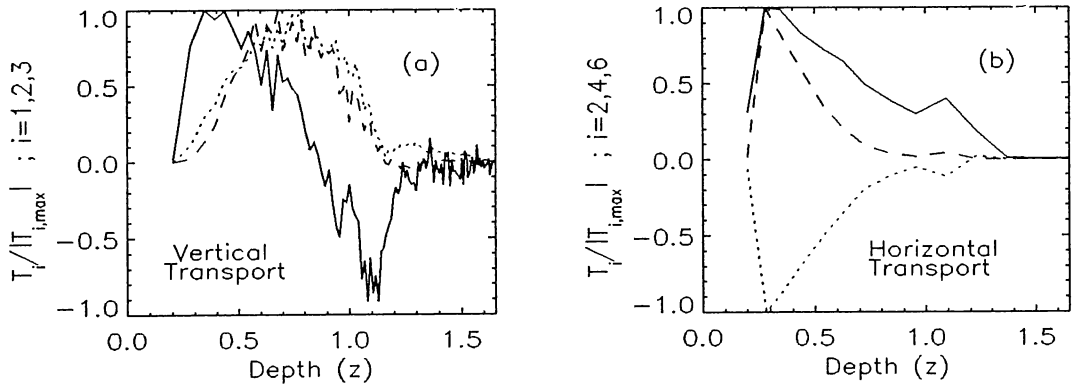

Figure 4. (a) The transfer coefficients T_1, T_2, and T_3 (solid, dotted, and dashed lines respectively) describing vertical transport as a function of depth for the higher resolution run at a time $t = 4.41$, which is about 1/5 of the convective turnover time. All are normalized with respect to their maximum values. (b) The normalized values of T_2, T_4, and T_6 (solid, dotted, and dashed lines) corresponding to horizontal transport for the same data set and time.

The first three nonzero horizontal and vertical transport coefficients are shown in Figure 4. Note that, for the horizontal transfer, only 14 levels in depth are shown out of the 105 available, so the curves are not complete, but do show a definite tendency for the coefficients, especially those of higher order, to decrease with depth. This decrease is expected because the characteristic horizontal velocity decreases with increasing density, although the relative decrease of the higher order coefficients is not obvious and indicates a relatively more diffusive behavior for the larger depths. The first vertical coefficient ($n = 1$) can be regarded as a typical advection velocity, and shows positive (downward) values throughout most of the convection zone and negative values in the upper part of the penetrative region. The secondary positive peak for the higher order coefficients just below the interface with the stable region indicates a typical scale at which downward plumes penetrate, then turn around and transport particles back upward. The relative magnitude of the coefficients as a function of order is shown in Figure 5 and is found to converge exponentially with increasing n for both vertical and horizontal transport. The relative dominance of the T_1 coefficient indicates again that the transport in the vertical direction is more advective than diffusive, although diffusion, as measured by the second coefficient, is non-vanishing.

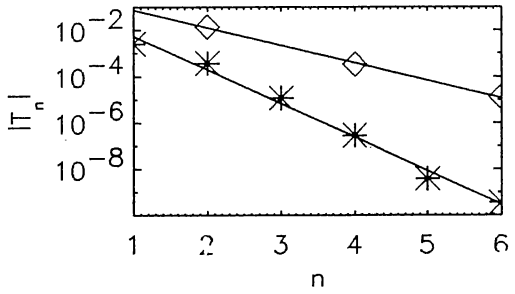

Figure 5. The typical magnitude for the transfer coefficients, $|T_n|$, averaged over depth for the higher resolution data set at time $t = 4.41$, as a function of order, n (plotted on log-linear axes). Results are shown for both vertical (asterisks) and horizontal (diamonds) transport. Recall that $T_n = 0$ by assumption for n odd in the horizontal case.

Other useful measures not related to the moments of the Green's function are obtained by summing the total particle fluxes across particular levels which arise from particle displacements of a specified length (Stull 1993). Thus, we define upward and downward "eddy fluxes" as follows:

$$F^{up}_{k\ell}(t) = \sum_{i=k}^{N_z} \sum_{j=0}^{k} G_{ij} \delta_{\ell(i-j)} \qquad (2.10)$$

and

$$F^{dn}_{k\ell}(t) = \sum_{i=0}^{k} \sum_{j=k}^{N_z} G_{ij} \delta_{\ell(j-i)}. \qquad (2.11)$$

These can be roughly associated with the scale, ℓ, of eddies that transport particles through the level k, although that identification is somewhat ambiguous because "eddies" of a given size would contribute to eddy fluxes at all smaller scales at time intervals which are not nearly multiples of the turnover time of that particular eddy. Still, they can give some useful information on the typical scale of mixing across a given level. We are interested in associating ℓ with a real physical length scale, so in calculating equations (2.10) and (2.11) from the simulation data, we use layers of constant volume rather than constant mass. It is therefore necessary to first evolve the particles to a statistically steady state before initializing the matrices to avoid the transient initial large downward flux of particles that occurs with stratified flows when volume shells are used.

Figure 6 illustrates typical results for $F^{up}_{k\ell}(t)$ and $F^{dn}_{k\ell}(t)$ as a function of eddy size, ℓ. Note that the upward flux tends to peak at somewhat smaller values of ℓ relative to the downward flux, leading to a net upward flux which is positive and negative respectively for small and large particle displacements. There is virtually no upward flux carried by eddies which exceed the size of the convection zone $\ell \geq 1$, although a significant amount of downward transport occurs on these scales. In other words, particles beginning in the convection zone often end up deep in the stable layer, but rarely does the opposite happen. The mixing intensity, $F_{up} + F_{dn}$ (not shown) peaks at fairly large eddies, typically about 70 - 80 % of the depth of the convection zone.

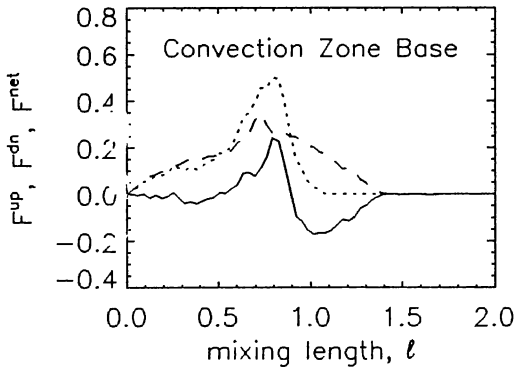

Figure 6. Shown are the upward, downward, and net particle flux (dotted, dashed, and solid lines respectively) after the particle concentration has reached a roughly steady state for a layer near the base of the convection zone (using the lower resolution data). The abscissa is the "eddy size", ℓ, as defined in equations (2.10) and (2.11).

CONCLUSIONS

We have investigated the chemical transport and mixing properties of convective MHD turbulence by applying a Greens-function-type formalism to numerical simulation data. This formalism has been developed by others (reviewed by Stull 1993) and has been used to study atmospheric flows (e.g. Ebert *et al.* 1989) , but to our

knowledge, has not yet been applied in an astrophysical context. The transilient or probability matrices which form the basis of the theory and which describe the time evolution of an arbitrary initial concentration of a passive scalar field are computed directly by following the trajectories of tracer particles, rather than solving additional differential equations as has been done previously (Ebert *et al.* 1989; Stull 1993). When computing moments and transfer coefficients, vertical displacements are measured in *mass layers* (vertical bins of constant mass) to take into account the anisotropic effects of stratification. The primary results for the flow simulations we have studied are as follows.

The mean square displacement of particles in both the horizontal and vertical directions closely follows a power law (at least for times less than a convection time scale) with an exponent greater than unity, characteristic of "anomalous" diffusion. In fact, the exponents are often close to the value 2, implying that the flows we have considered are much more advective than diffusive. In the convection zone, this is likely to be the case due to the influence of coherent structures such as vertical plumes and coherent, converging and diverging horizontal flows. Advective transport in the stable layer could arise from particle trapping in traveling gravity waves (Knobloch & Merryfield 1992), although the wave field in the stable layer should be dominated by standing waves as a result of the reflective lower boundary conditions. To shed further light on these issues, it is important to redo the simulations with boundary conditions on the lower boundary which allow gravitational wave radiation, or alternatively, to see how sensitive the nature of transport in the stable layer is to the layer's width.

The normalized fourth moment, the kurtosis, of each column of the transilient matrix is found to be relatively invariant with time, at least for some levels, so it provides a good measure of how an injection of particles at a given level spreads out initially with time. Significant deviations both greater and less than 3 (which is expected for diffusion) are observed. Typical values are largest just above the base of the convection zone, especially for downward transport, indicating the importance of intermittency - i.e. extreme events with large displacements are common relative to diffusion. This implies that penetrative convection could play an important role in transporting small amounts of Lithium and other light elements from the convection zone to a depth in the radiative interior where they are efficiently burned, and may therefore be a significant factor in determining the Li depletion observed on the solar surface.

Transport coefficients are calculated and are found to converge exponentially with order, n. The relative dominance of the $n = 1$ (advective) coefficient suggests again that the flows studied here are more advective than diffusive. It would be interesting to apply the present formalism to more turbulent flows to see if this conclusion remains true as the forcing is increased.

On average, downward transport occurs on larger scales than does upward transport, with a net flux that is typically positive for smaller "eddys" and negative (downward) on length scales comparable to and larger than the depth of the convection zone.

Acknowledgements. This work was supported under NASA SPTP and NCAR ASP grants, and with funding from the SOI/MDI project.

REFERENCES

1. Brandenburg, A., Jennings, R. L., Nordlund, A., Rieutord, M., Stien, R. F., & Tuominen, I. 1995a, J. Fluid Mech., in press

1. Brandenburg, A., Mesch, M.S., Zweibel, E.G., & Toomre, J. 1995b, in preparation

1. Bouchaud, J.-P., & Georges, A. 1990, Phys. Rep 195, 127

1. Ebert, E. E., Schumann, U., & Stull, R. B. 1989, J. Atmos. Sci., 46, 2178

1. Knobloch, E. & Merryfield, W. J. 1992, Ap. J. 401, 196

1. Stull, R. B. 1993, Boundary Layer Meteorology, 62, 21

1. Van Beijeren, H. 1982, Rev. Mod. Phys. 54, 196

Poster Group 6:

Internal Rotation